Supplementary Materials for

Improving the Stability of Solar Cells Using Metal-Organic Frameworks

Vagif Nevruzoglu[1#], Selçuk Demir[2#*], Gokcehan Karaca[3], Murat Tomakin[3], Nuray Bilgin[1], Fatih Yilmaz[2]

[1] Recep Tayyip Erdoğan University, Faculty of Engineering, Department of Energy Systems Engineering, Rize, Turkey.

[2] Recep Tayyip Erdoğan University, Faculty of Arts and Sciences, Department of Chemistry, Rize, Turkey.

[3] Recep Tayyip Erdoğan University, Faculty of Arts and Sciences, Department of Physic, Rize, Turkey.

L1: Biphenyl-4,4'-dicarboxylate

L2: 2,2'-bipyridine-5,5'-dicarboxylate

[#]These authors contributed equally to this work. [*]*e-mail:* selcuk.demir@erdogan.edu.tr

Results of Zr-L1 MOF

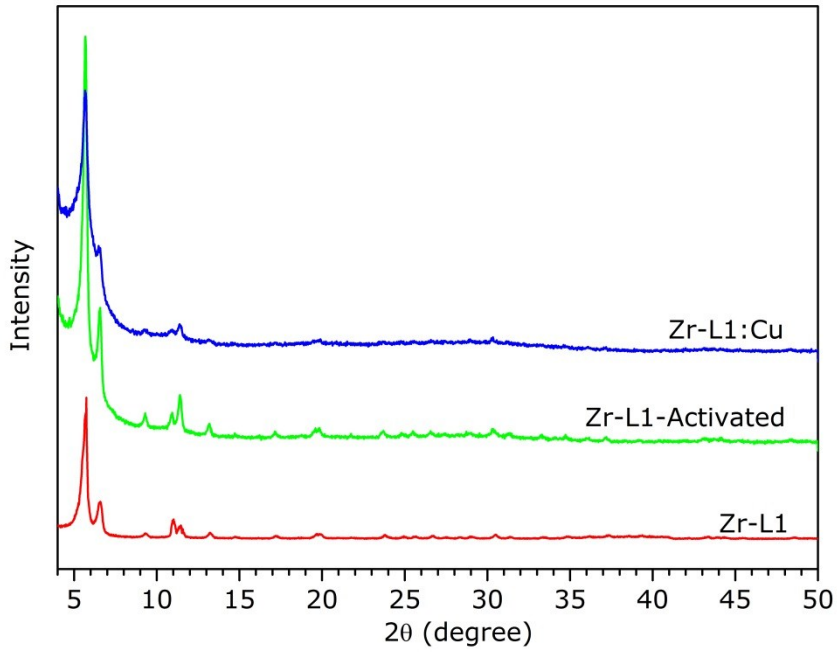

Figure S1. XRD patterns of the Zr-L1, Zr-L1-activated and Zr-L1:Cu MOFs

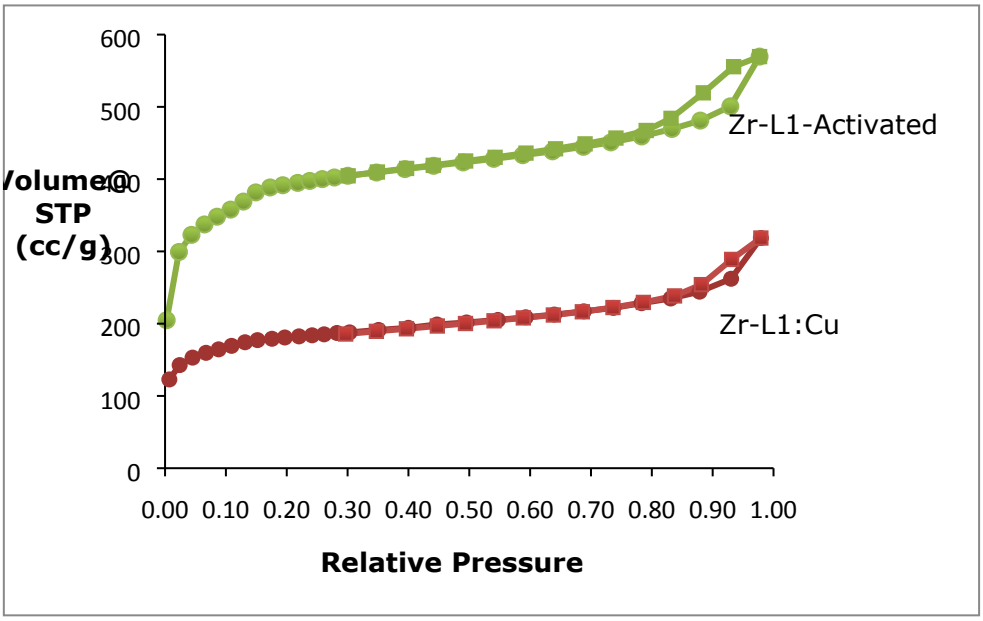

Figure S2. Adsorption (sphere) and desorption (square) isotherms of the Zr-L1-activated and Zr-L1:Cu MOFs.

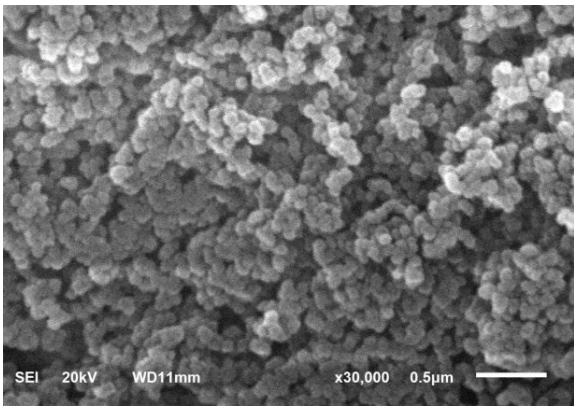

a) SEM image of the Zr-L1-activated MOF

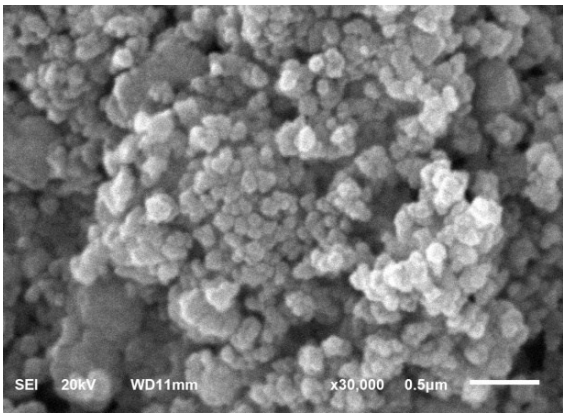

b) SEM image of the Zr-L1:Cu MOF

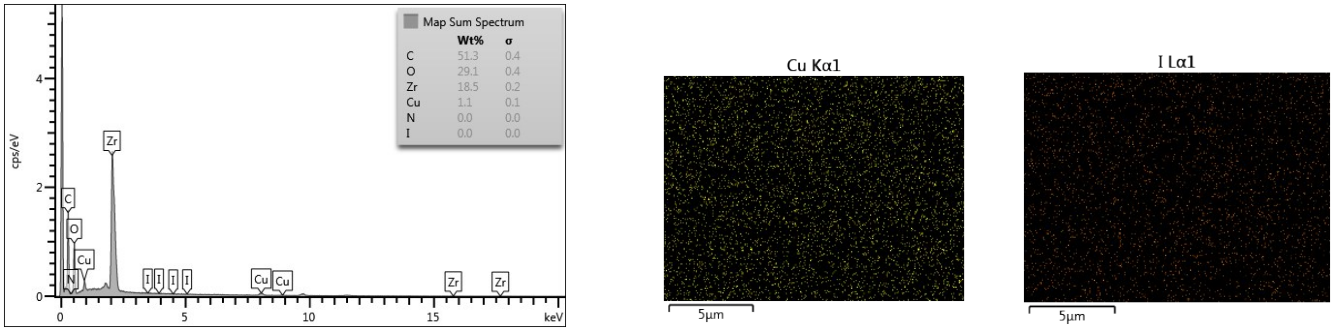

c) EDX results of the Zr-L1:Cu MOF

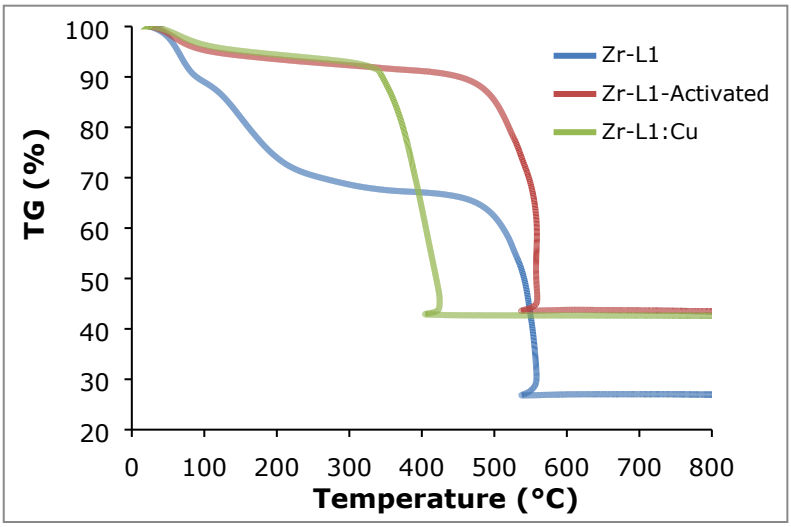

d) TG curves of the Zr-L1, Zr-L1-activated and Zr-L1:Cu MOFs under dynamic air atmosphere

Figure S3. SEM images of the Zr-L1-activated MOF (a), and Zr-L1:Cu (b), EDX results of the Zr-L1:Cu MOF (c) and TG curves of the Zr-L1, Zr-L1-activated and Zr-L1:Cu MOFs under dynamic air atmosphere (d).

Results of Zr-L2 MOF

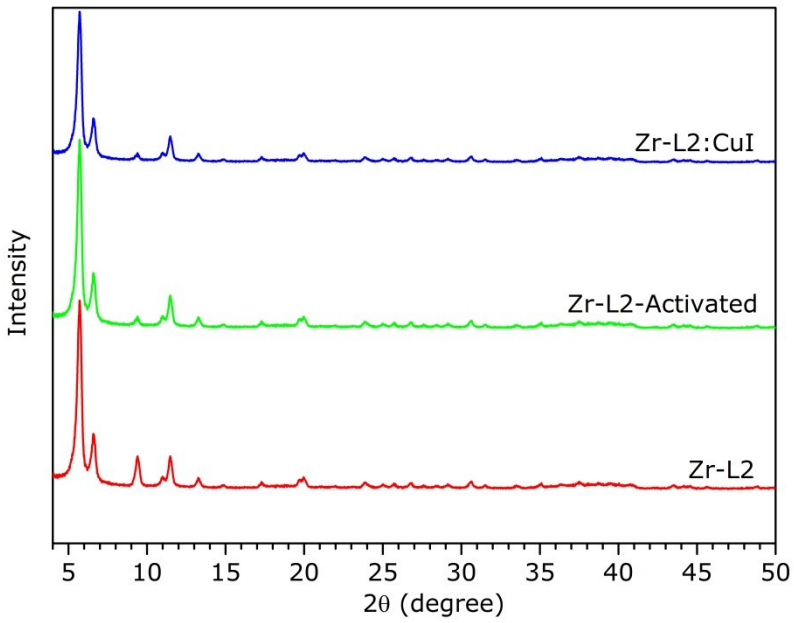

Figure S4. XRD patterns of the Zr-L2, Zr-L2-activated and Zr-L2:Cu MOFs

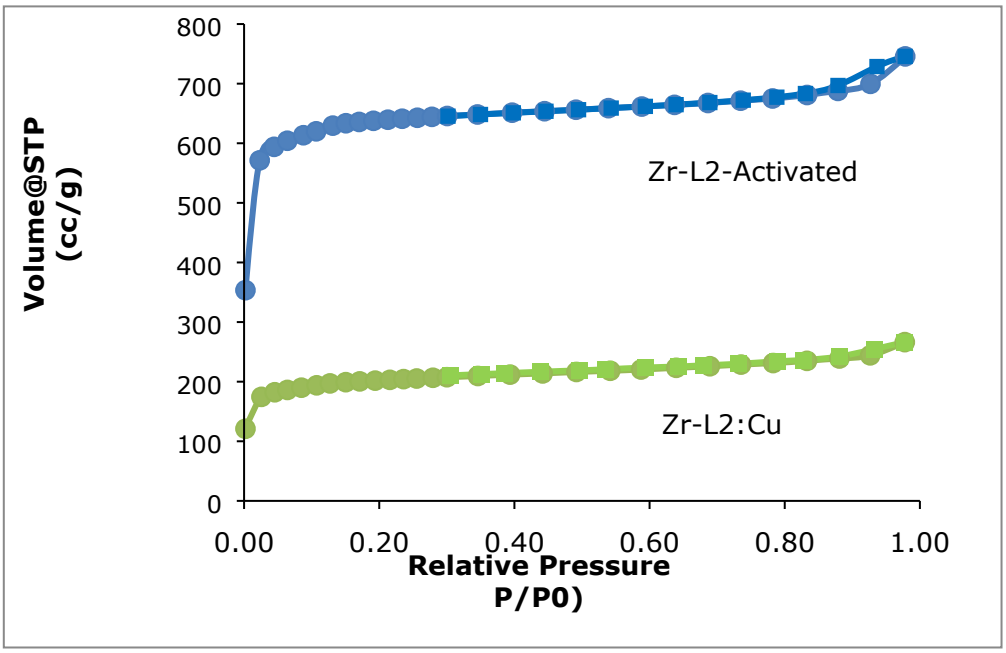

Figure S5. Adsorption (sphere) and desorption (square) isotherms of the Zr-L2-activated and Zr-L2:Cu MOFs.

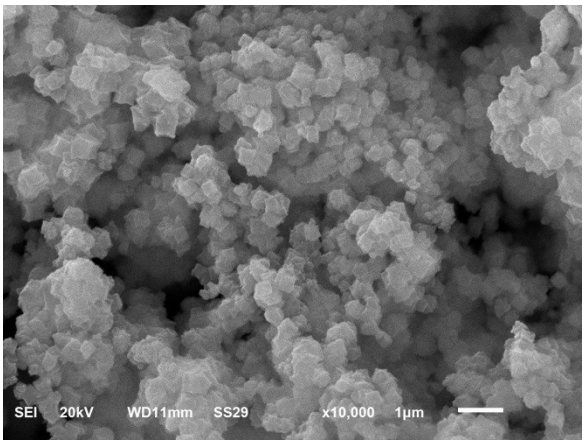

a) SEM image of the Zr-L2-activated MOF

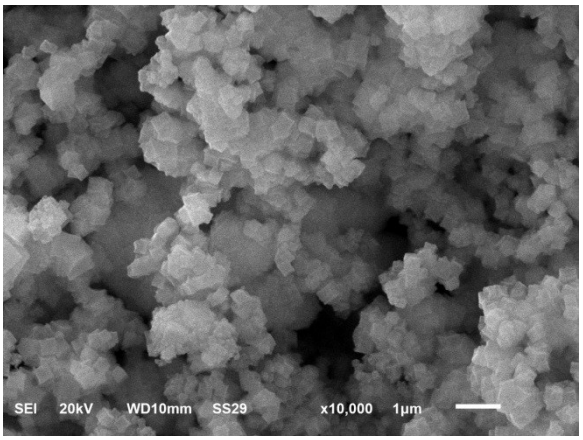

b) SEM image of the Zr-L2:Cu MOF

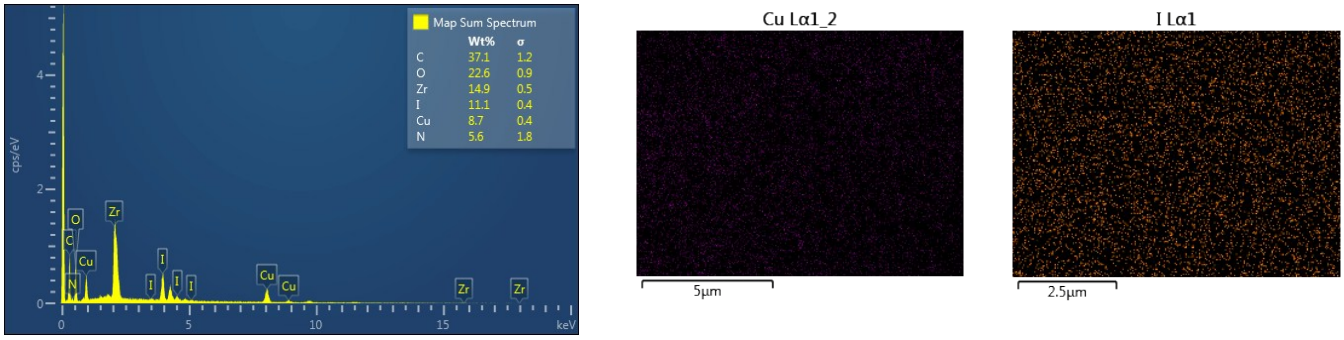

c) EDX results of the Zr-L2:Cu MOF

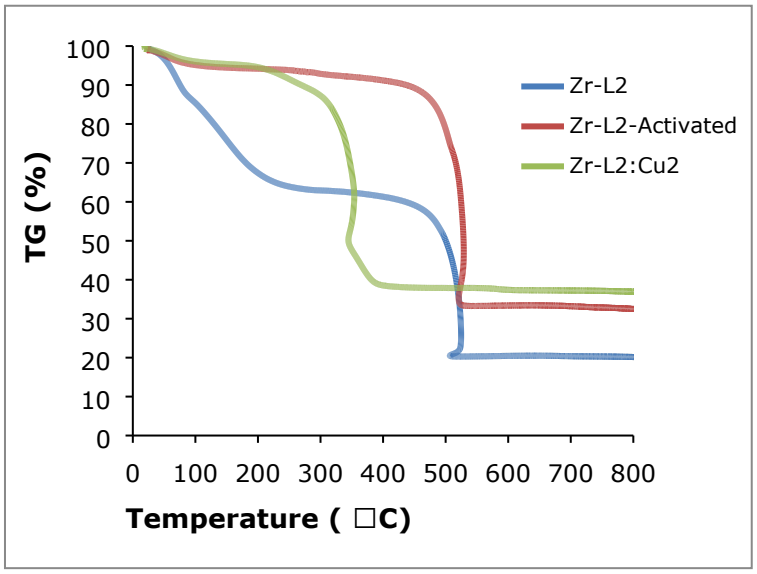

d) TG curves of the Zr-L2, Zr-L2-activated and Zr-L2:Cu MOFs under dynamic air atmosphere

Figure S6. SEM images of the Zr-L2-activated MOF (a), and Zr-L2:Cu (b), EDX results of the Zr-L2:Cu MOF (c) and TG curves of the Zr-L2, Zr-L2-activated and Zr-L2:Cu MOFs under dynamic air atmosphere (d).

Results of Zr-L1L2 MOF

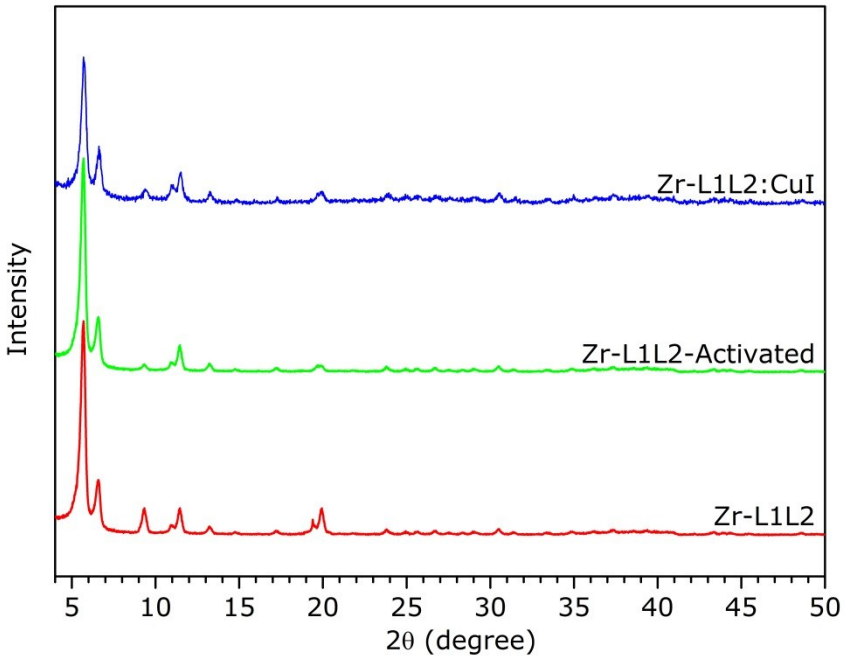

Figure S7. XRD patterns of the Zr-L1L2, Zr-L1L2-activated and Zr-L1L2:Cu MOFs

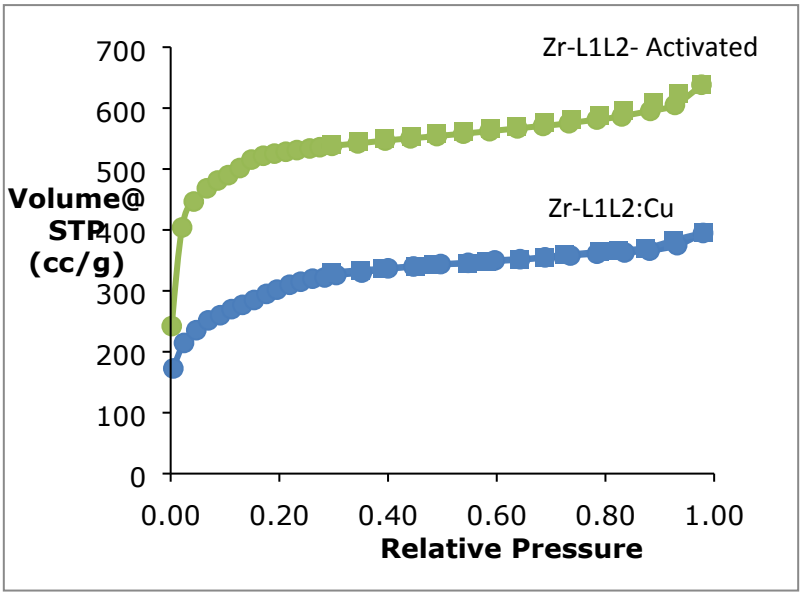

Figure S8. Adsorption (sphere) and desorption (square) isotherms of the Zr-L1L2-activated and Zr-L1L2:Cu MOFs.

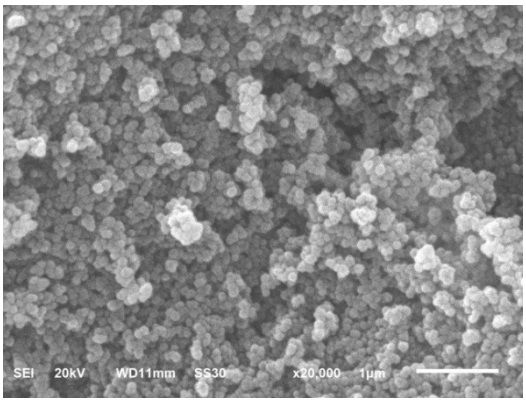

a) SEM image of the Zr-L1L2-activated MOF

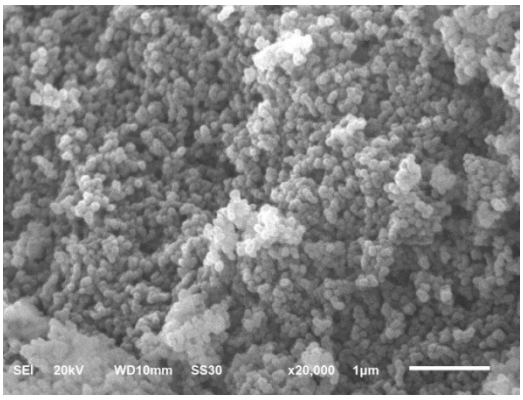

b) SEM image of the Zr-L1L2:Cu MOF

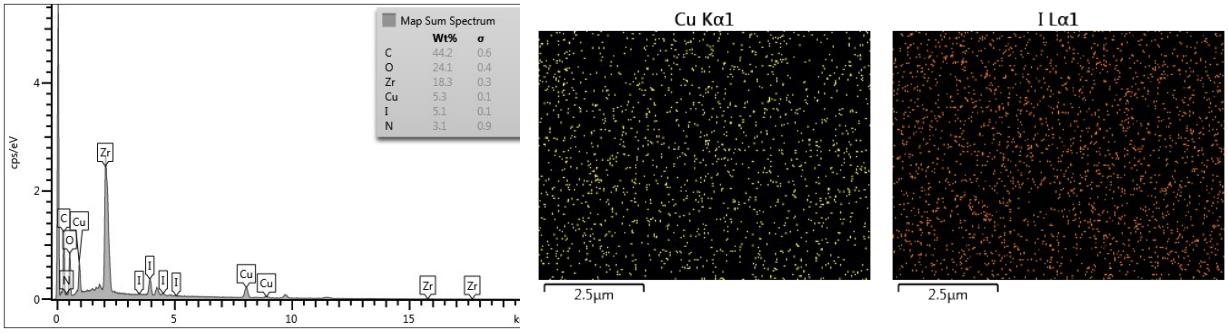

c) EDX results of the Zr-L1L2:Cu MOF

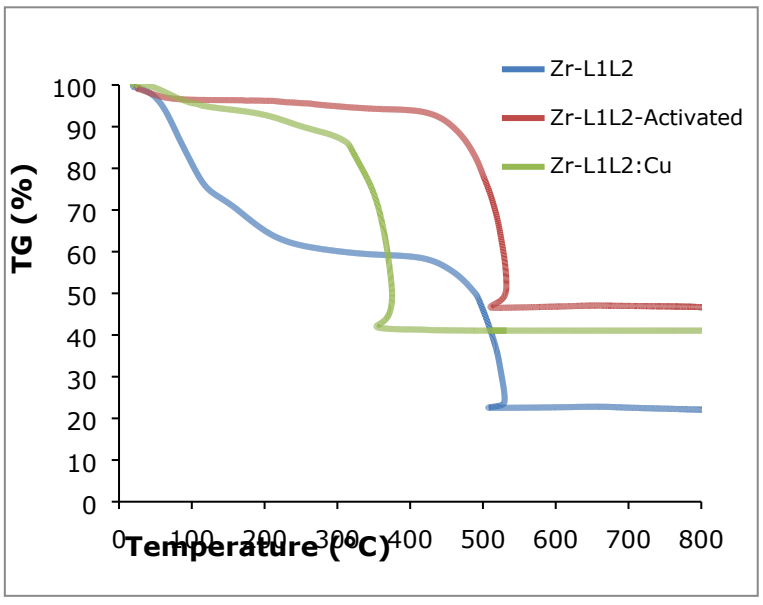

d) TG curves of the Zr-L1L2, Zr-L1L2-activated and Zr-L1L2:Cu MOFs under dynamic air atmosphere

Figure S9. SEM images of the Zr-L1L2-activated MOF (a), and Zr-L1L2:CuI (b), EDX results of the Zr-L1L2:Cu MOF (c) and TG curves of the Zr-L1L2, Zr-L1L2-activated and Zr-L1L2:Cu MOFs under dynamic air atmosphere (d).

Table S1. Elemental composition* and some physical properties of the Zr-MOFs

	Mol. Formula	M_A (g/mol)	C (%Wt)	H (%Wt)	N (%Wt)	Zr (%Wt)	Cu (%Wt)	H_2O (%, TG)	BET (m^2/g)	Particle size (nm)
Zr-L1-activated	$Zr_6O_4(OH)_4(C_{14}H_8O_4)_6 \cdot 6H_2O$	2228.7	46.69 (45.27)	2.67 (2.89)	-	23.43 (24.56)	-	5.70 (4.84)	1405	70-100nm
Zr-L1:Cu	$Zr_6O_4(OH)_4(C_{14}H_8O_4)_6(CuI)_{0.5} \cdot 6H_2O$	2324.0	42.83 (43.41)	2.99 (2.78)	-	23.05 (23.55)	1.10 (1.37)	5.10 (4.65)	1226	70-100nm
Zr-L2-activated	$Zr_6O_4(OH)_4(C_{12}H_6N_2O_4)_6 \cdot 8H_2O$	2276.6	37.92 (37.98)	2.41 (2.48)	7.38 (7.38)	17.20 (24.04)	-	5.70 (6.32)	2360	200-300
Zr-L2:Cu	$Zr_6O_4(OH)_4(C_{12}H_6N_2O_4)_6(CuI)_6 \cdot 18H_2O$	3599.5	23.65 (24.02)	2.24 (2.13)	4.71 (4.67)	14.90 (15.21)	9.10 (10.59)	8.70 (9.00)	1392	200-300
Zr-L1L2-activated	$Zr_6O_4(OH)_4(C_{14}H_8O_4)_3(C_{12}H_6N_2O_4)_3 \cdot 8H_2O$	2270.7	40.24 (41.26)	2.69 (2.75)	4.27 (3.70)	22.72 (24.10)	-	5.40 (6.34)	1921	70-120
Zr-L1L2:Cu	$Zr_6O_4(OH)_4(C_{14}H_8O_4)_3(C_{12}H_6N_2O_4)_3(CuI)_3 \cdot 6H_2O$	2806.0	33.71 (33.39)	2.17 (2.08)	3.74 (3.00)	18.36 (19.51)	5.30 (6.79)	4.20 (3.85)	1235	50-120

*Calculated values were given in the parentheses.

Thermal Properties

In order to determine the amount of occluded solvents as well as information about the thermal stabilities of the prepared metal-organic frameworks, we performed thermogravimetric analysis (TGA) under a dynamic air atmosphere. Though the as-prepared materials (Zr-L1, Zr-L2, and Zr-L1L2) exhibit significant weight losses (35-45%) before their thermal decomposition, dried materials (Zr-L1-activated, Zr-L2-activated, and Zr-L1L2-activated) display limited weight losses. This indicates successful activation (Figures S3d, S6d, and S9d). The weight losses in the as-prepared TGA curves were attributed to occluded solvent molecules within the pores. Furthermore, the experimental and calculated water content is compatible with the corresponding activated (dried) samples (Table S1). However, the calculated final residues (ZrO_2 + CuO) show some discrepancy. The residue values are between ZrO_2 + CuO and ZrO_2 + Cu_2O. Thus, it is likely that some of the Cu ions were not oxidized during the TGA measurement and remain as Cu_2O. Additionally, any defects present

can increase these deviations. The as-prepared and activated materials are stable up to approximately 400-450 °C. Furthermore, metalated samples display much lower thermal stability when compared to the activated samples. We attribute this to the impregnated copper ions catalyzing the decomposition of the MOFs. A lower thermal stability of metalated MOFs has precedence in the literature [ref. 37, SI]."

Thickness of Solar Cells

It is known that the serial resistance is one of the reasons which affect the yield of a solar cell. Thus, in order to determine the effect of thickness of Cu-MOF layer onto the resistance, we prepared layers with different thicknesses between two ITO substrates as in "preparation of solar cell" section, and measured I-V characteristics. As a result, the thickness of the Cu-MOF layers with a suitable resistance was determined as 30-150 nm for this work. The prepared system produced noise for the layer thicker than 150 nm and leakage current for the layer thinner than 30 nm. Consequently, we chose 50 nm as a working thickness.

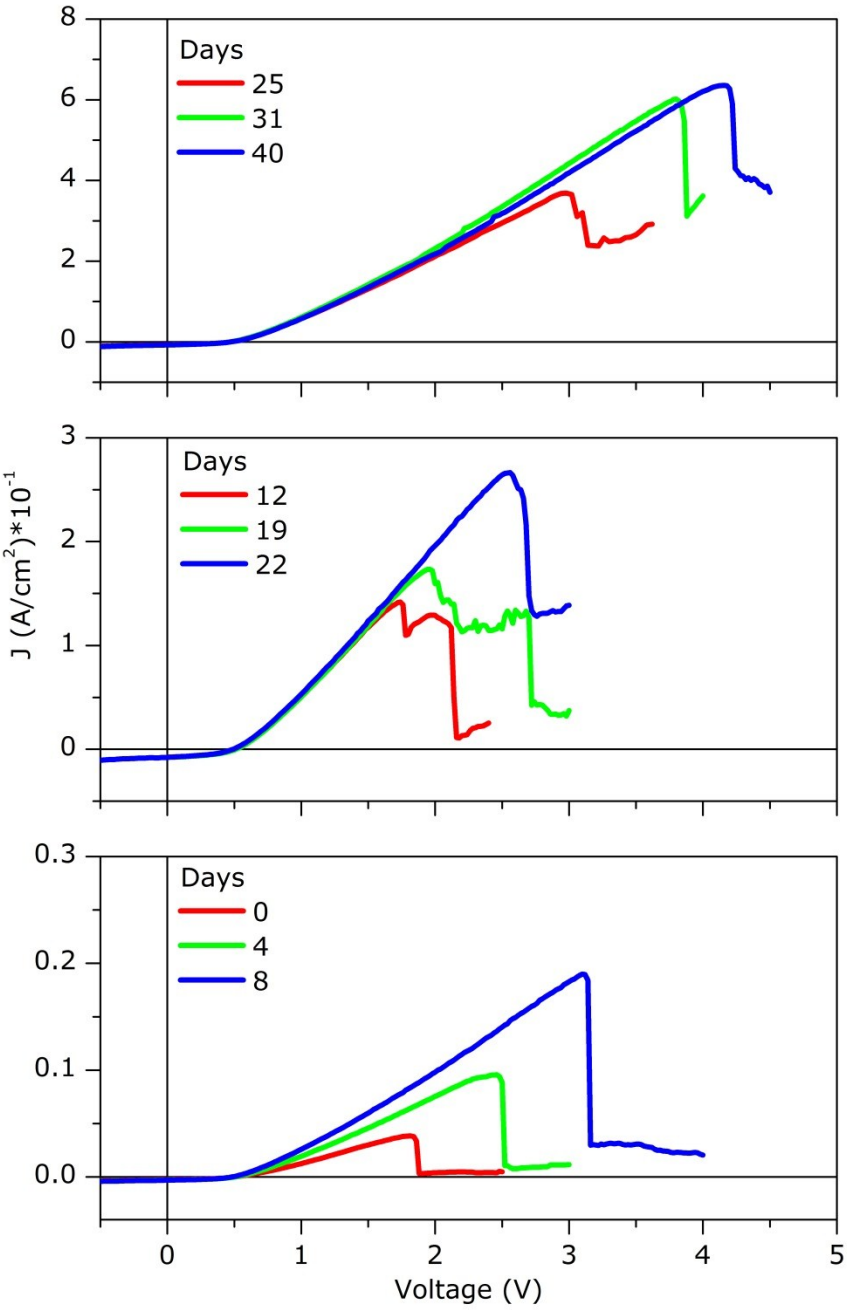

Figure S10. *J-V* curves of the Zr-L1L2:Cu/$Cu_{2-x}S$/CdS cell measured on different days.

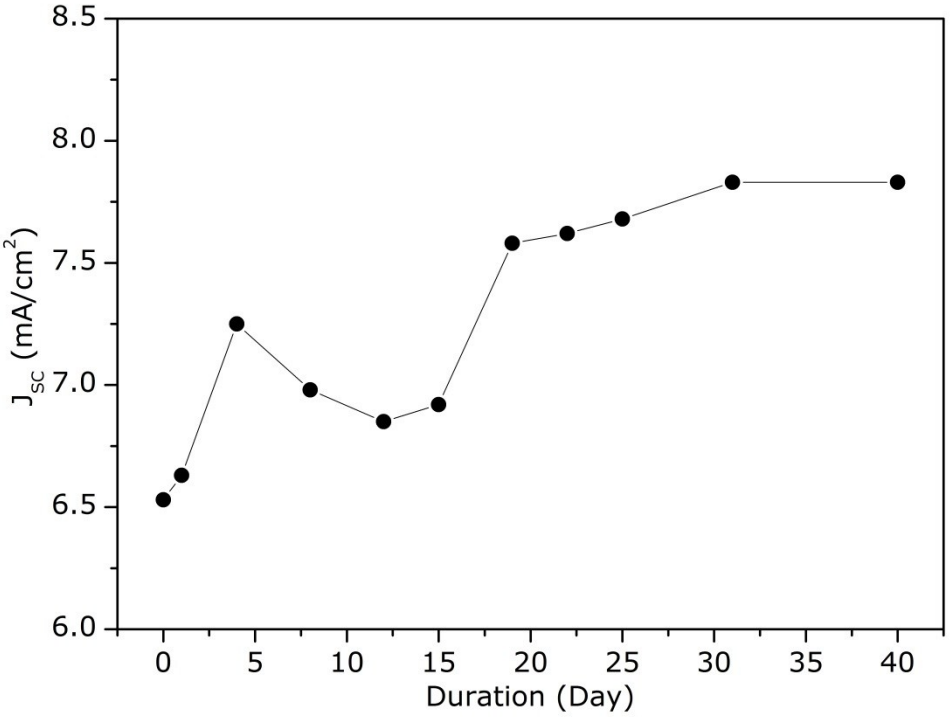

Figure S11. J_{sc} curve of the Zr-L1L2:Cu/$Cu_{2-x}S$/CdS cell measured between the MOF strips (see Figure 1- model c)

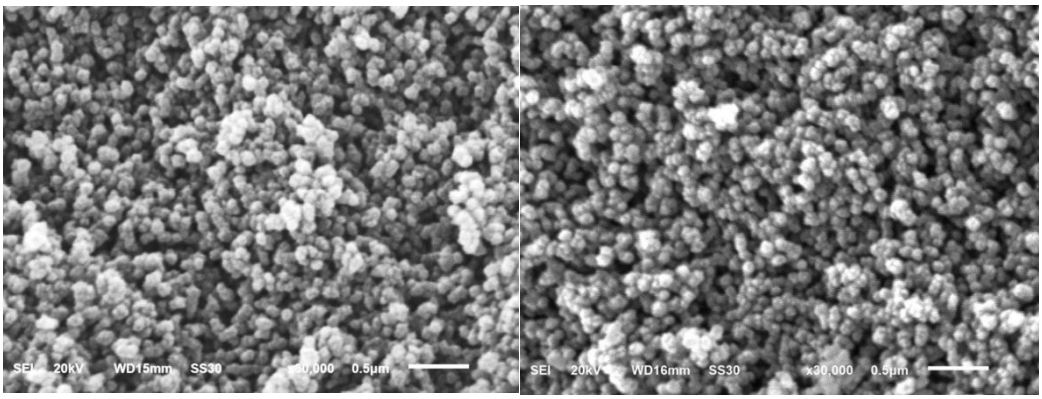

Figure S12 a. SEM image of the Zr-L1-activated MOF before and after irradiation under solar simulator.

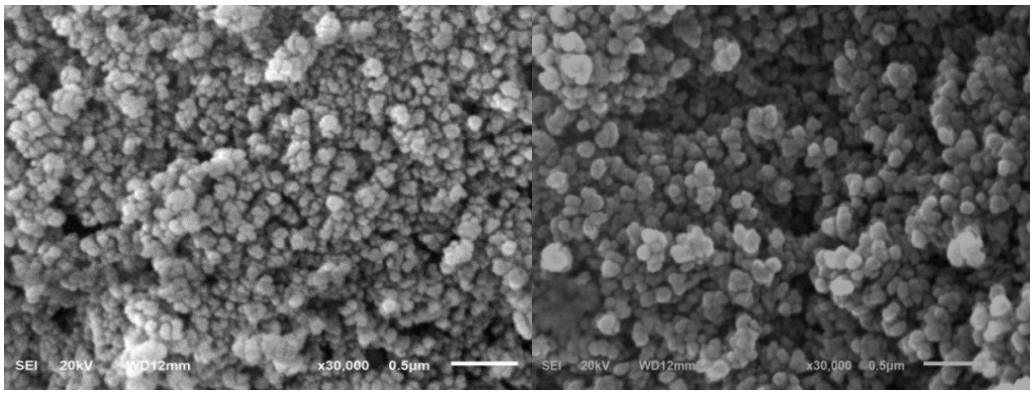

Figure S12 b. SEM image of the Zr-L1:Cu (1.1% Cu) MOF before and after irradiation under solar simulator.

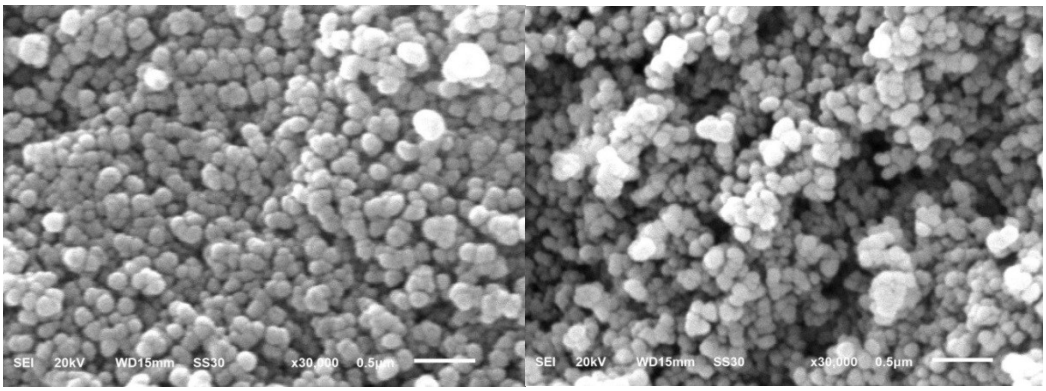

Figure S12 c. SEM image of the Zr-L1L2:Cu (5.30% Cu) MOF before and after irradiation under solar simulator.

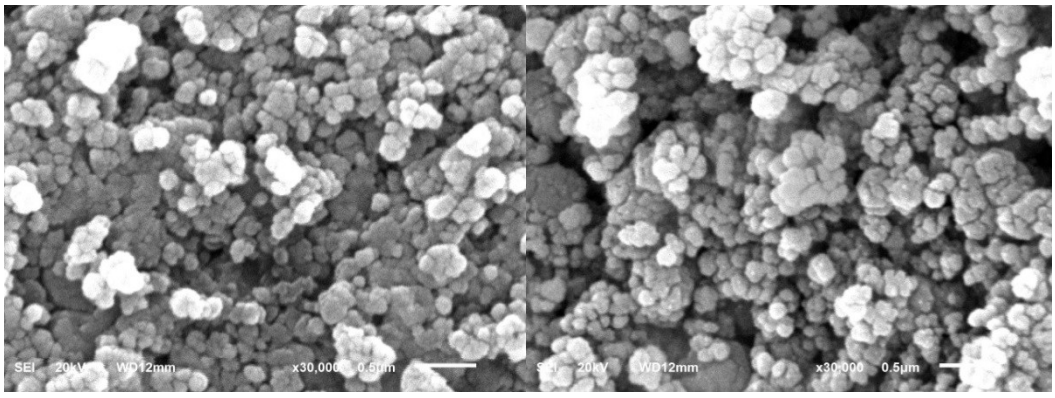

Figure S12 d. SEM image of the Zr-L2:Cu (9.10% Cu) MOF before and after irradiation under solar simulator.

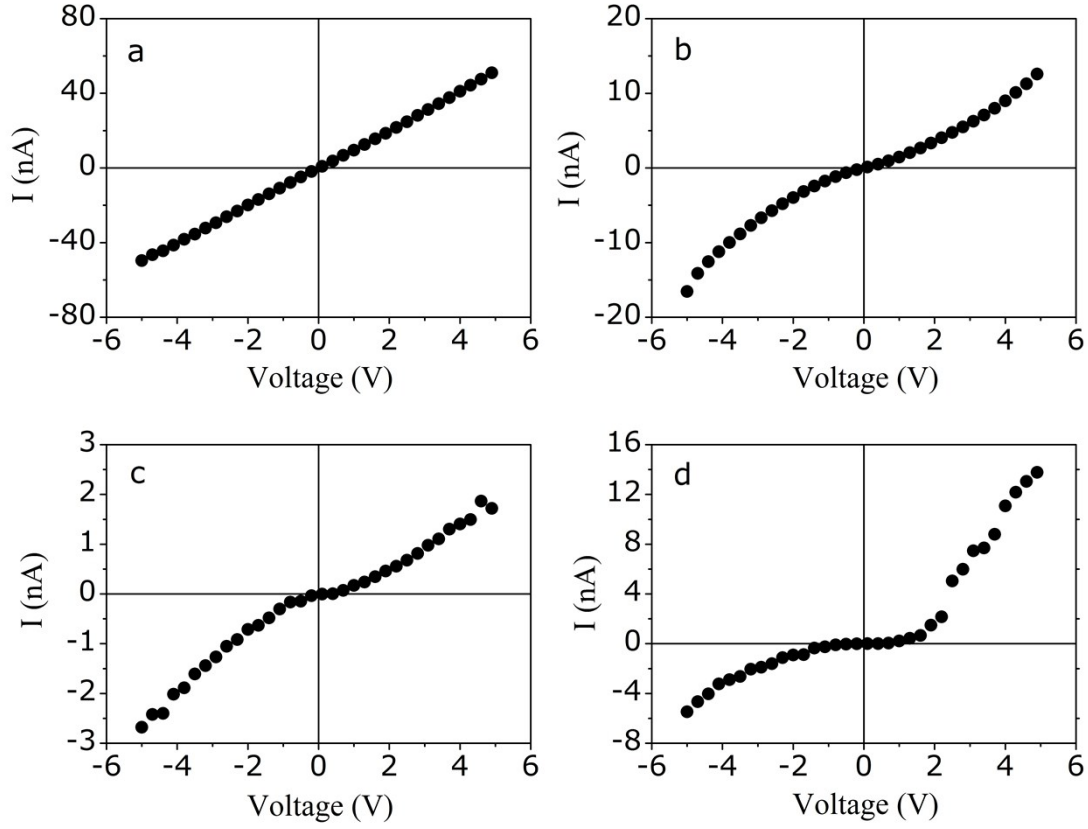

Figure S13. I-V curves of the Zr-L1L2:Cu MOF layers prepared on CdS single crystals. a) after preparation; b) after one week at room conditions; c) after annealing for 40 minutes at 100 °C; d) after annealing for 40 minutes at 180 °C.